LETTER

doi:10.1038/nature11672

The root of branching river networks

J. Taylor Perron[1], Paul W. Richardson[1], Ken L. Ferrier[1] & Mathieu Lapôtre[2]

Branching river networks are one of the most widespread and recognizable features of Earth's landscapes and have also been discovered elsewhere in the Solar System[1,2]. But the mechanisms that create these patterns and control their spatial scales are poorly understood. Theories based on probability[3–5] or optimality[3,6–8] have proven useful[9], but do not explain how river networks develop over time through erosion and sediment transport. Here we show that branching at the uppermost reaches of river networks is rooted in two coupled instabilities: first, valleys widen at the expense of their smaller neighbours, and second, side slopes of the widening valleys become susceptible to channel incision. Each instability occurs at a critical ratio of the characteristic timescales for soil transport and channel incision. Measurements from two field sites demonstrate that our theory correctly predicts the size of the smallest valleys with tributaries. We also show that the dominant control on the scale of landscape dissection in these sites is the strength of channel incision, which correlates with aridity and rock weakness, rather than the strength of soil transport. These results imply that the fine-scale structure of branching river networks is an organized signature of erosional mechanics, not a consequence of random topology.

Observers have long recognized that branching river networks, in which tributaries merge in the downstream direction, are a fundamental outcome of erosion by flowing water. Early field observations led to conceptual models in which hierarchical drainage networks result from progressive integration of initially separate drainages through divide migration and stream capture[10,11]. More than a century of study of erosional mechanics has culminated in numerical models that produce landscapes dissected by branching river networks[12–14] and lend some support to the early conceptual models, but a physically based theory that explains the form of tributary networks has proven elusive[15].

One of the main reasons for this shortcoming is that there is no clear consensus about what such a theory should be able to predict. Early efforts to identify unique geometric characteristics of natural river networks[11,16,17] failed when the proposed scaling laws were subsequently shown to apply to all hierarchical networks, riverine or otherwise[3,4,18]. This fuelled a broader class of studies based on principles other than erosional mechanics, including probabilistic models of topologically random networks[3–5] and optimality arguments based on energy dissipation or entropy[3,6–8]. Such studies have provided new insights into the structure of natural river networks[9], but cannot directly relate river network form to the erosional mechanisms that shape the topography: we know what the skeleton of a landscape looks like, but not how it grows.

Thus, despite progress in characterizing the geometry of drainage networks and modelling landscape evolution, it remains unclear how the form of drainage networks records the dominant factors that shape landscapes, such as bedrock properties, tectonic deformation, climate and life. Here we use a simplified model to show that branching tributary networks form through two coupled instabilities, and propose that the scale of the smallest valleys with tributaries is a signature of this process. We then present field measurements from two sites with drainage networks that differ considerably in scale, and show that both are consistent with our theory. This comparison reveals how the spatial structure of river networks records fundamental geological and environmental factors such as rock type and rainfall.

To identify characteristic scales in tributary networks, we mapped the valley networks in two landscapes with similar erosion processes but different scales of fluvial dissection (Fig. 1). The Allegheny Plateau

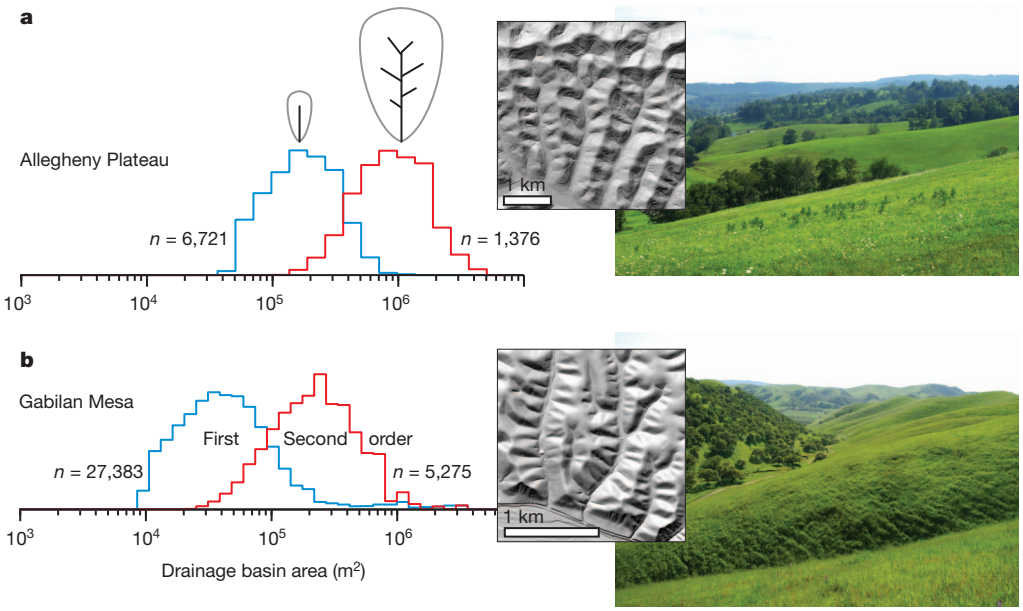

Figure 1 | Properties of the study sites. **a**, The Allegheny Plateau, Pennsylvania; **b**, Gabilan Mesa, California. Left, area distributions of first- and second-order drainage basins, with inset sketches showing examples of first- and second-order basins. Coloured lines are histograms with counts weighted by drainage basin area to compensate for the greater abundance of smaller basins. Insets at centre, shaded relief maps of small portions of the study sites generated from laser altimetry, with vegetation filtered out. Right, photographs showing views from the tops of ridgelines, with first-order valleys in the near distance. See Methods for data sources.

[1]Department of Earth, Atmospheric and Planetary Sciences, Massachusetts Institute of Technology, Cambridge, Massachusetts 02139, USA. [2]École et Observatoire des Sciences de la Terre, Université de Strasbourg, F-67084 Strasbourg, France.

©2012 Macmillan Publishers Limited. All rights reserved

in southwest Pennsylvania and northern West Virginia consists of horizontally bedded Permian sandstone with minor lenses of limestone, siltstone, shale and coal[19]. Land cover is dominantly pasture and deciduous forest, and mean annual precipitation is 105 cm. Gabilan Mesa is an elevated area on the eastern margin of California's Salinas Valley where rivers have incised into nearly horizontally bedded Pliocene and Pleistocene conglomerate, sandstone and siltstone[20]. The Mesa is an oak savanna that receives 32 cm of rain per year. Both landscapes are shaped dominantly by soil creep due to bioturbation, particularly animal burrowing, and by river channel incision that, in the small drainage basins studied here, is episodic[21], occurring at estimated intervals of years to many decades.

We mapped the valley network over a large area of each landscape (Methods). We then applied the Horton-Strahler stream ordering scheme[11,16] to identify first-order drainage basins (those with no tributaries) and second-order drainage basins (those with at least one first-order tributary) (Fig. 1). The upstream areas drained by basins of a given order are log-normally distributed around a well-defined modal value (Fig. 1). Moreover, we find that the modal drainage areas of first- and second-order basins in the Allegheny Plateau and Gabilan Mesa differ considerably. The smallest basins with tributaries are typically four times larger in the Allegheny Plateau, despite the similar appearance of the landscape (Fig. 1). We seek an explanation for this fundamental scale difference.

Valleys bounded by smooth ridgelines emerge in soil-mantled landscapes from a competition between river channel incision, which amplifies topographic perturbations, and soil creep, which damps perturbations. The extent of valley incision can also be limited by a threshold for runoff production or surface erosion[22], but we make the simplification that soil creep is the dominant effect, an assumption supported by previous analyses[21,23]. The smoothing effect of soil creep can be characterized with a diffusion time, $t_{diff} = L^2/D$, where L is a horizontal length scale and D is the soil transport coefficient (in $m^2\,yr^{-1}$). Channel incision can be characterized by an advection time that describes the rate at which changes in elevation propagate through the drainage network, $t_{adv} = L^{1-2m}/K$, where m is a constant and K is a channel incision rate coefficient (in $m^{1-2m}\,yr^{-1}$). The ratio t_{diff}/t_{adv}, which describes the strength of channel incision relative to soil creep at a chosen scale L, is analogous to a Péclet number, $Pe = KL^{1+2m}/D$ (refs 21, 23).

We suggest that branching valley networks will develop at a finer scale in landscapes where channel incision is stronger relative to soil creep. To test this idea, we used a landscape evolution model (Methods) to simulate the development of a ridgeline bounded by two incising channels for many different values of Pe. Each simulation formed drainage basins extending from the bounding channels up towards the drainage divide (Supplementary Fig. 5). The length scale L was chosen to be the half-width of the ridgeline, which roughly equals the length of the largest basins (Fig. 2a, inset). (Throughout this study, L is taken to be the length of a drainage basin, or the length of a slope on which a drainage basin may develop.) From the final, equilibrium topography in each experiment, we measured the drainage areas of the basins. A plot of normalized drainage area versus Pe for all the simulations (Fig. 2a) reveals a transition at $250 < Pe < 300$. For $Pe < 250$, drainage basins have a uniform size. For $Pe > 300$, the distribution of basin size is bimodal, with each basin either extending all the way from a lowering boundary to the central drainage divide, or extending only part way to the divide and occupying a small space between larger basins. Nearly all of the larger basins for $Pe > 300$ developed tributaries (Supplementary Fig. 5).

We interpret this transition in landscape form in terms of a stability diagram (Fig. 2a). At $Pe < 250$, an array of parallel, uniformly sized basins is a stable configuration: additional numerical experiments confirmed that if any one basin in such a configuration is perturbed by increasing its drainage area, the topographic divides separating the enlarged basin from its neighbours will migrate back towards the

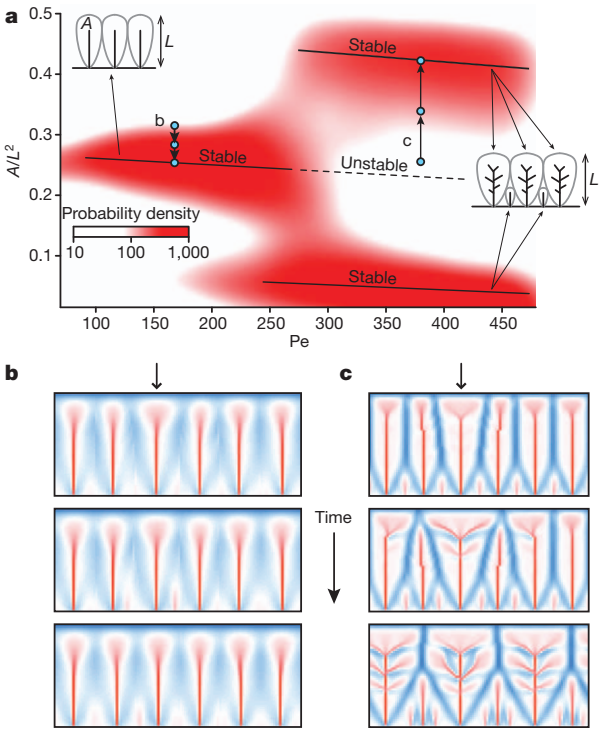

Figure 2 | Branching instability in valley networks. **a**, Stability diagram for first- and second-order drainage basins as a function of Péclet number, Pe. Insets illustrate the definitions of ridgeline half-width, L, and basin area, A. Background colour (see key) indicates probability density distribution of drainage basins generated in numerical experiments, which partly reflects variable initial conditions (Methods). Paths with blue points and arrows trace the evolution of the numerical experiments in **b** and **c**, which illustrate the response of an array of parallel valleys to a perturbation in which one valley (marked with an arrow) is enlarged slightly. Colours in **b** and **c** denote drainage area, with blues corresponding to ridgelines and reds to valleys.

centre of the enlarged basin, such that it shrinks back to the size of its neighbours (Fig. 2b). At $Pe > 300$, an array of parallel, uniformly sized basins is unstable: enlarging the drainage area of any one basin causes the topographic divides to continue to migrate away from the centre of the enlarged basin, such that it widens at the expense of its neighbours (Fig. 2c). This instability propagates through the landscape until all drainage basins have either grown or shrunk to reach one of the two stable sizes. Supplementary Fig. 3 shows several drainage basins in Gabilan Mesa that may have experienced this instability. This transformation of the drainage network is comparable to an effect observed in laboratory analogue experiments[24], and may explain the uniform aspect ratios of basins that drain to linear boundaries[25].

The qualitative explanation for the critical value of Pe concerns the feedbacks that operate when a basin is enlarged. The increase in drainage area increases channel discharge, and therefore channel incision rate. Faster incision further deepens the basin, driving the surrounding ridgelines towards neighbouring basins and enlarging the drainage area—a positive feedback. Competing against this is a negative feedback in which deeper valleys with a sharper "V" shape are filled in faster by diffusive soil creep. For $Pe > \sim 300$, the positive feedback is stronger.

This instability explains the enlargement of some of the basins, but it does not explain why the enlarged basins develop tributaries on their side slopes (Fig. 2c). To determine why the tributaries grow, we performed a second experiment in which we subjected an inclined, planar surface with a prescribed Péclet number (intended to mimic the side slopes of a drainage basin) to a series of small-amplitude perturbations with a range of wavelengths, and measured the growth or decay rate of the perturbations (Fig. 3). The length scale L used to calculate Pe was

©2012 Macmillan Publishers Limited. All rights reserved

chosen to be the horizontal length of this sloping surface, which is the length of the incipient valleys. For Pe $<\sim$60, perturbations of all wavelengths decay, and no tributary valleys form. At Pe $\approx$ 60, wavelengths of roughly one-third of the slope length become unstable, and grow into incipient tributary valleys. The range of unstable wavelengths widens as Pe increases above this critical value. A similar wavelength selection has been inferred in analytical studies of incipient channelization under sheet flow[26,27].

To relate this instability to tributary valleys like those in Fig. 2c, we calculate Péclet numbers for the side slopes of drainage basins with and without tributaries in the numerical model solutions, using the horizontal lengths of the basin side slopes as L (Fig. 3 inset). This comparison confirms that the difference between valleys with and without tributaries is whether Pe for their side slopes is greater than or less than the critical value of $\sim$60. For example, the side slopes of the first-order basins in Fig. 2b have Pe = 12, whereas those of the second-order basins in Fig. 2c have Pe = 75. Thus, the basin-widening instability shown in Fig. 2 is accompanied by the formation of tributary valleys because the lengthening side slopes exceed the critical Pe for growth of incipient valleys.

Together, these two instabilities provide an explanation for the characteristic branching pattern of fine-scale tributary networks. In addition, our theory makes a testable prediction: second-order drainage basins should have Péclet numbers that exceed the critical value of $\sim$300 (Fig. 2a), regardless of the absolute spatial scale of the landscape. To test this prediction, we calculated Pe for drainage basins in the Allegheny Plateau and Gabilan Mesa. This requires measurements of K/D, m and drainage basin length, L, each of which can be estimated from topographic data. K/D and m have been estimated[21] for representative sites in each landscape from an independent analysis of the topography (Supplementary Table 2). Combining these values with our measurements of L (Methods), we compiled frequency distributions of Pe (Fig. 4). Unlike the drainage area distributions in Fig. 1, which differ between sites by a factor of four, the Pe distributions are quite similar. The critical range of $250 <$ Pe < 300 (Fig. 2) falls between the modal values for first- and second-order basins in both landscapes, consistent with the prediction that most second-order basins should exceed this range, whereas most first-order basins should not. The match is slightly better for the Allegheny Plateau, whereas the gap between the modes occurs at approximately $300 <$ Pe < 350 for Gabilan Mesa, but this difference is small compared with the scale discrepancy in Fig. 1. In addition, most first-order basins in both landscapes exceed the critical value of Pe $\approx$ 60 for the development of incipient valleys (Figs 3 and 4). Thus, drainage networks in both the Allegheny Plateau and Gabilan Mesa are consistent with our proposed mechanism for tributary network development, despite their difference in spatial scale.

This result implies that the ratio of coefficients describing the long-term rates of channel incision and soil creep, K/D, can be estimated from a drainage basin's stream order and size. Because m is typically $\sim$0.5 (ref. 28, Supplementary Table 2), Pe $\approx KL^2/D$ as a rule of thumb. Thus, $K/D \approx \mathrm{Pe}_n/L^2$, where Pe_n is the modal Péclet number for a basin of order n (from Fig. 4, for example, $\mathrm{Pe}_2 \approx 600$). With this approach, it may be possible to use remote imagery to help calibrate long-term erosion laws, a result with promise for both terrestrial and planetary landscapes. The specific expressions presented here only apply to low-order, steady-state drainage basins shaped by regolith creep and ephemeral channel incision. Nonetheless, the principle that stream order and basin size provide a proxy for long-term process rates may also apply to higher-order drainage basins and landscapes shaped by different hillslope and channel erosion mechanisms. We show in the Supplementary Information that the branching mechanism documented in Figs 2 and 3 occurs even with different erosion and transport laws, provided that channel incision depends on drainage area and regolith transport depends on slope.

To understand how the geological, climatic and biological characteristics of a landscape control the scale of the drainage network, we performed an additional calculation. Gabilan Mesa is made of weaker rocks than the Allegheny Plateau, receives less rainfall in a more seasonal distribution, and has vegetation dominated by grasses rather than forest; it also has larger K/D (Supplementary Table 2) and therefore a finer-scale drainage network (Fig. 1). We determined K and D independently to discover whether this larger ratio reflects stronger channel incision, less mobile soil, or both. Combining long-term erosion rates inferred from cosmogenic ^{10}Be in river sediment (Methods, Supplementary Table 1) with surveys of hillslope topography, we calculated D for the Allegheny Plateau and Gabilan Mesa, and divided D by D/K to obtain K (Methods, Supplementary Table 2). This calculation clearly shows that the main difference between the sites is the strength of channel incision: whereas D differs by only 25% (and is actually larger at Gabilan Mesa, the opposite of what would be expected if D were responsible for the scale difference), the channel incision rate factor for a reference drainage area, KA_{ref}^m, is roughly seven times larger at Gabilan Mesa (Supplementary Table 2). The magnitudes and uniformity of the soil diffusivities measured here are consistent with measurements from other landscapes in Mediterranean to humid climates[29], and probably reflect similar soil mechanical properties and bioturbation intensities. There are two likely and

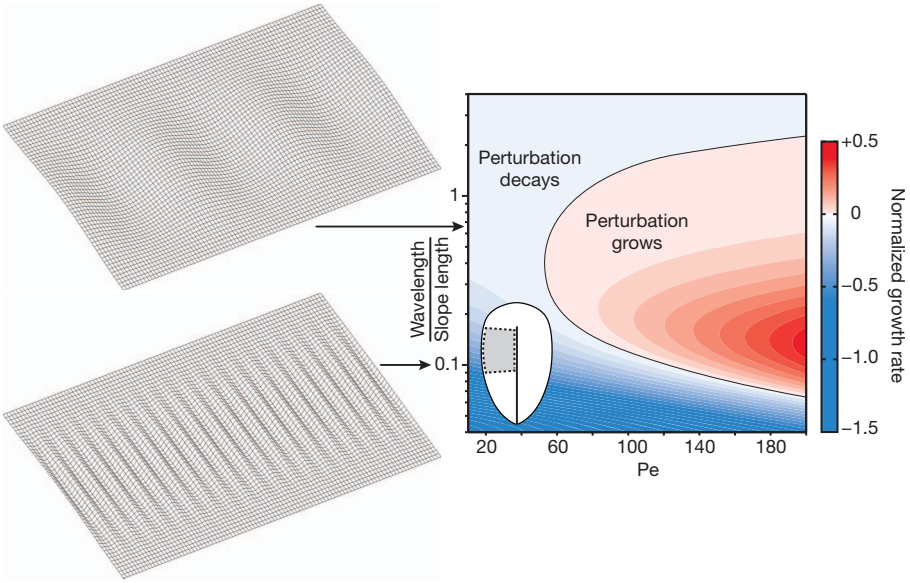

Figure 3 | Growth rates of incipient valleys on inclined slopes. Left, wire mesh plots showing vertically exaggerated examples of sinusoidal perturbations on inclined, planar slopes. Right, normalized growth rate (colour coded) of sinusoidal perturbations as a function of Péclet number, Pe, and aspect ratio (wavelength divided by slope length). Normalized growth rate is proportional to the fractional rate of change of the standard deviation of surface elevation after the background slope has been removed. Contour interval is 0.05, and the black line is the zero contour. Inset, illustration of the hypothetical position of such a slope within a larger drainage basin.

©2012 Macmillan Publishers Limited. All rights reserved

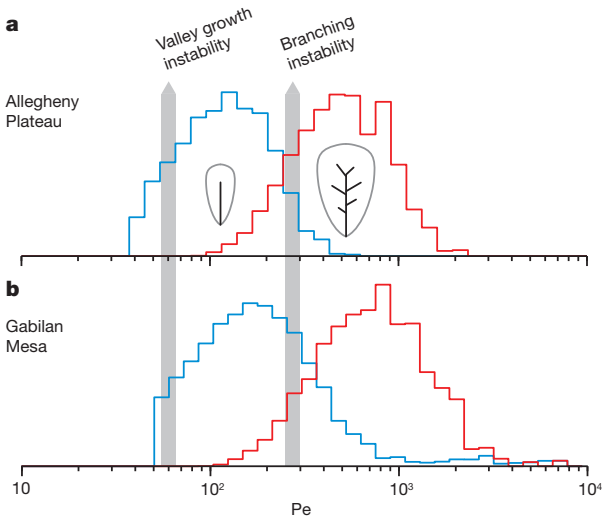

Figure 4 | Péclet number distributions of first- and second-order drainage basins in the study sites. a, Allegheny Plateau; **b**, Gabilan Mesa. Coloured lines are histograms with counts weighted by drainage basin area to compensate for the greater abundance of smaller basins. Inset sketches are examples of first- and second-order basins. Grey bars indicate critical values of Pe for valley growth (Fig. 3) and branching (Fig. 2). Basins analysed are the same as in Fig. 1.

non-exclusive explanations for the difference in channel incision: first, the weaker rocks at Gabilan Mesa are easier to erode; and second, highly seasonal rainfall and sparser vegetation at Gabilan Mesa promote runoff and inhibit infiltration, such that larger surface flows occur at a given drainage area and mean rainfall rate. The broader implication of this result is that the finely branched tips of river networks, which form both the skeleton and the circulatory system of Earth's landscapes, carry a fundamental signature of rock strength, climate and life. A remaining challenge is to further quantify this signature by relating specific materials, mechanisms and conditions to the rate constants used to describe landscape evolution over geologic time.

METHODS SUMMARY

Topographic analysis. We identified valleys in laser altimetry data as areas of anomalously positive contour curvature (Supplementary Fig. 1). We then traced valley networks over a larger region using a steepest-descent flow routing procedure and a drainage area threshold based on the curvature criterion, and assigned Strahler stream orders to these networks (Supplementary Fig. 2). Drainage basin areas, A, are determined just upstream of the junction with a higher-order link. We approximated[22] drainage basin length as $L \approx \sqrt{3A}$, and calculated the Péclet number as $\mathrm{Pe} = (K/D)(3A)^{m+\frac{1}{2}}$.

Landscape evolution model. The model[21,23] solves an equation for the time evolution of an elevation surface due to rock uplift or boundary lowering, channel incision and downslope soil transport. We solved this equation forward in time with a finite difference method[23] on a rectangular grid with periodic x boundaries, lowering y boundaries, and a low-relief, randomly rough initial surface. We varied the Péclet number by varying K/D and performed 1,600 runs with different initial conditions to determine the probability densities in Fig. 2a.

Cosmogenic nuclides. We estimated long-term erosion rates by measuring the concentration of cosmogenic ^{10}Be in quartz grains in stream sediment (Supplementary Table 1) and converting these concentrations to surface erosion rates based on rates of ^{10}Be production and decay.

Calculation of *K* and *D*. We assumed steady state hillslope topography and calculated the soil transport coefficient as $D = -E/\nabla^2 z_h$, where E is the surface erosion rate determined from cosmogenic ^{10}Be and $\nabla^2 z_h$ is the Laplacian of elevation on hilltops, which has been measured from laser altimetry[21] (Supplementary Table 2). The channel incision coefficient K was calculated by dividing D by previous estimates[21] of D/K, and the channel incision coefficient for a reference drainage area, KA_{ref}^{m}, was calculated with previous estimates[21] of m and $A_{ref} = 10^4\ \mathrm{m}^2$ (Supplementary Table 2).

Full Methods and any associated references are available in the online version of the paper.

Received 16 April; accepted 27 September 2012.

1. Mars Channel Working Group. Channels and valleys on Mars. *Geol. Soc. Am. Bull.* **94,** 1035–1054 (1983).
2. Tomasko, M. G. *et al.* Rain, winds and haze during the Huygens probe's descent to Titan's surface. *Nature* **438,** 765–778 (2005).
3. Leopold, L. B. & Langbein, W. B. The concept of entropy in landscape evolution. *Prof. Pap. US Geol. Surv.* **500-A,** 1–20 (1962).
4. Shreve, R. L. Infinite topologically random channel networks. *J. Geol.* **75,** 178–186 (1967).
5. Howard, A. Simulation of stream networks by headward growth and branching. *Geogr. Anal.* **3,** 29–50 (1971).
6. Howard, A. Theoretical model of optimal drainage networks. *Wat. Resour. Res.* **26,** 2107–2117 (1990).
7. Sun, T., Meakin, P. & Jøssang, T. Minimum energy dissipation model for river basin geometry. *Phys. Rev. E* **49,** 4865–4872 (1994).
8. Rigon, R., Rinaldo, A., Rodriguez-Iturbe, I., Bras, R. L. & Ijjasz-Vasquez, E. Optimal channel networks: a framework for the study of river basin morphology. *Wat. Resour. Res.* **29,** 1635–1646 (1993).
9. Rodriguez-Iturbe, I. & Rinaldo, A. *Fractal River Basins: Chance and Self-Organization* (Cambridge Univ. Press, 2001).
10. Gilbert, G. K. *Report on the Geology of the Henry Mountains* (US Govt Printing Office, 1877).
11. Horton, R. E. Erosional development of streams and their drainage basins: hydrophysical approach to quantitative morphology. *Bull. Geol. Soc. Am.* **56,** 275–370 (1945).
12. Willgoose, G., Bras, R. L. & Rodriguez-Iturbe, I. Results from a new model of river basin evolution. *Earth Surf. Process. Landf.* **16,** 237–254 (1991).
13. Howard, A. D. A detachment-limited model of drainage basin evolution. *Wat. Resour. Res.* **30,** 2261–2286 (1994).
14. Tucker, G. E. & Slingerland, R. Drainage basin responses to climate change. *Wat. Resour. Res.* **33,** 2031–2047 (1997).
15. Dunne, T. Formation and controls of channel networks. *Prog. Phys. Geogr.* **4,** 211–239 (1980).
16. Strahler, A. N. Quantitative analysis of watershed geomorphology. *Trans. Am. Geophys. Union* **38,** 913–920 (1957).
17. Schumm, S. A. Evolution of drainage systems and slopes in badlands at Perth Amboy, New Jersey. *Geol. Soc. Am. Bull.* **67,** 597–646 (1956).
18. Kirchner, J. W. Statistical inevitability of Horton's laws and the apparent randomness of stream channel networks. *Geology* **21,** 591–594 (1993).
19. Berg, T. M. *et al. Geologic Map of Pennsylvania* (Pennsylvania Geological Survey, 1980).
20. Durham, D. L. Geology of the southern Salinas Valley area, California. *Prof. Pap. US Geol. Surv.* **819,** 1–111 (1974).
21. Perron, J. T., Kirchner, J. W. & Dietrich, W. E. Formation of evenly spaced ridges and valleys. *Nature* **460,** 502–505 (2009).
22. Montgomery, D. R. & Dietrich, W. E. Channel initiation and the problem of landscape scale. *Science* **255,** 826–830 (1992).
23. Perron, J. T., Dietrich, W. E. & Kirchner, J. W. Controls on the spacing of first-order valleys. *J. Geophys. Res.* **113,** F04016, http://dx.doi.org/10.1029/2007JF000977 (2008).
24. Bonnet, S. Shrinking and splitting of drainage basins in orogenic landscapes from the migration of the main drainage divide. *Nature Geosci.* **2,** 766–771 (2009).
25. Hovius, N. Regular spacing of drainage outlets from linear mountain belts. *Basin Res.* **8,** 29–44 (1996).
26. Smith, T. R. & Bretherton, F. P. Stability and the conservation of mass in drainage basin evolution. *Wat. Resour. Res.* **8,** 1506–1529 (1972).
27. Izumi, N. & Parker, G. Inception of channelization and drainage basin formation: upstream-driven theory. *J. Fluid Mech.* **283,** 341–363 (1995).
28. Snyder, N. P., Whipple, K. X., Tucker, G. E. & Merritts, D. J. Landscape response to tectonic forcing: digital elevation model analysis of stream profiles in the Mendocino triple junction region, northern California. *Geol. Soc. Am. Bull.* **112,** 1250–1263 (2000).
29. Fernandes, N. F. & Dietrich, W. E. Hillslope evolution by diffusive processes: the timescale for equilibrium adjustments. *Wat. Resour. Res.* **33,** 1307–1318 (1997).

Supplementary Information is available in the online version of the paper.

Acknowledgements This study was supported by the US National Science Foundation Geomorphology and Land Use Dynamics programme through award EAR-0951672 to J.T.P. and by the US Department of Defense through a National Defense Science and Engineering Graduate Fellowship to P.W.R. J.T.P. is a Scholar in the Canadian Institute for Advanced Research (CIFAR). The authors thank T. Clifton and G. Chmiel for assistance with sample preparation, and the Orradre family of San Ardo, California, and numerous landowners in Greene County, Pennsylvania, for granting access to their land.

Author Contributions J.T.P. conceived of the study, performed the numerical modelling, and wrote the paper. J.T.P., P.W.R. and K.L.F. conducted the fieldwork. P.W.R. processed the ^{10}Be samples, and P.W.R. and K.L.F. analysed the ^{10}Be data. J.T.P. and M.L. performed the topographic analyses.

Author Information Reprints and permissions information is available at www.nature.com/reprints. The authors declare no competing financial interests. Readers are welcome to comment on the online version of the paper. Correspondence and requests for materials should be addressed to J.T.P. (perron@mit.edu).

©2012 Macmillan Publishers Limited. All rights reserved

METHODS

Topographic analysis. We mapped valley networks in the central Gabilan Mesa (GM) in California, between the towns of King City and San Miguel, and the Waynesburg Hills area of the Allegheny Plateau (AP) in Pennsylvania and West Virginia, in the Dunkard Creek, Fish Creek and South Fork Ten Mile Creek watersheds, using a combination of airborne laser altimetry and the US National Elevation Dataset (NED). Laser altimetry for GM was acquired and processed by the National Center for Airborne Laser Mapping (NCALM), and laser altimetry for AP was produced by the PAMAP program of the Pennsylvania Department of Conservation and Natural Resources. Both laser altimetry data sets were filtered to remove vegetation and gridded to a horizontal point spacing of 1 m.

We first used the laser altimetry to map valley networks over subregions of roughly 25 km^2. We mapped valleys rather than channels to focus on the long-term topographic signature of channel incision rather than the most recent episodes (particularly since the latter may have been influenced by human land use). To objectively map the valley network, we used a procedure that identifies valleys as areas with anomalously convergent topography, as defined below, and then uses flow routing to bridge any gaps in the resulting map. The steps in this procedure are illustrated in Supplementary Fig. 1. First, elevations were smoothed with a Gaussian filter with a standard deviation of 10 m (GM) or 20 m (AP) to reduce fine-scale roughness (Supplementary Fig. 1a). Contour curvature (Supplementary Fig. 1b) was then calculated as[30,31]:

$$\kappa_c = \frac{\left(\frac{\partial z}{\partial y}\right)^2 \frac{\partial^2 z}{\partial x^2} - 2\frac{\partial z}{\partial x}\frac{\partial z}{\partial y}\frac{\partial^2 z}{\partial x \partial y} + \left(\frac{\partial z}{\partial x}\right)^2 \frac{\partial^2 z}{\partial y^2}}{\left(\left(\frac{\partial z}{\partial x}\right)^2 + \left(\frac{\partial z}{\partial y}\right)^2\right)^{\frac{3}{2}}} \quad (1)$$

Following a recently proposed procedure[32,33], we identified valleys as areas in which contour curvature is sufficiently positive that it deviates from the approximately Gaussian frequency distribution of curvature over most of the terrain. Specifically, we defined valleys as clusters of points with κ_c greater than two standard normal quantiles above the mean, which is the value at which the frequency distribution of κ_c begins to deviate substantially from a Gaussian distribution (Supplementary Fig. 1c). To exclude small, scattered local minima on hillslopes that satisfy the curvature criterion, we additionally required that the clusters be at least 10 m^2 in size. To exclude depressions in nearly planar topography (such as on alluviated valley floors) that are not part of the valley network, we required that clusters include at least one point with a drainage area (calculated with the D-infinity algorithm[34]) greater than two standard normal quantiles above the mean.

Applying the curvature criterion produced a binary map of pixel clusters that lie within areas of strongly convergent topography (Supplementary Fig. 1d). We then routed flow over the entire landscape using a steepest-descent algorithm[35], identified the pixel in each cluster with the largest drainage area, and traced flow paths downslope from these pixels to the boundaries of the elevation grid. The resulting network of clusters joined by flow paths (Supplementary Fig. 1e) contained some parallel flow paths in areas with subtly varying slope directions, because the steepest-descent algorithm is insensitive to changes in flow direction of less than 45°. Parallel flow paths were merged (Supplementary Fig. 1f) by applying a morphological closing operation[36] with a disk-shaped structuring element with a radius of 10 m. The resulting skeleton was thinned to a network one pixel wide and pruned to remove spurs less than 10 m long (Supplementary Fig. 1g).

We then used this laser altimetry-based drainage network to calibrate a procedure for mapping the drainage network over a much larger area using coarser elevation data. In this procedure, the steepest-descent flow-routing algorithm was applied to the 10 m resolution (GM) or 30 m resolution (AP) NED over the same area covered by the laser altimetry, the drainage network was identified as the set of points with drainage area greater than a minimum value, A_{min}, and the network was pruned to remove spurs less than 20 m (GM) or 30 m (AP) in length. The laser altimetry-based network was then compared with the NED-based network. For each study site, we identified the value of A_{min} that maximized the number of valleys appearing as first-order links in both networks, and found A_{min} = 10,000 m^2 for GM and 50,400 m^2 for AP. Using these values, we mapped the drainage networks over larger geographic areas with the NED, increasing our sample size from tens of drainage basins to several thousand, and assigned Strahler stream orders[11,16] to the networks. For each first-order or second-order link in a network, we identified the associated drainage basin as the area that drains to the point on the link just upstream of the junction with a higher-order link. Comparison of the laser altimetry-based valley network with NED-based drainage basin boundaries (Supplementary Fig. 2) indicates that the calibrated analysis of NED elevation data correctly identifies the boundaries of most first-order and second-order drainage basins, despite the coarser resolution. The mapped valley network corresponds to areas that have experienced significant channel incision over geologic time, but does not necessarily coincide with the extent of the currently active channel network[37]. Recent episodes of channel incision may extend further upslope than the long-term average in some locations (such as the small gullies visible in Supplementary Fig. 2), while in others, valleys that have experienced significant long-term incision may lack currently active channels.

To transform drainage basin areas into the lengths, L, used to calculate the Péclet number, Pe, we used the well-known observation that drainage basin area scales with the square of basin length to a good approximation over many orders of magnitude in basin size[38]. It has been found[22] that $L \approx \sqrt{3A}$, with the factor of $\sqrt{3}$ describing the non-square shape of drainage basins. Thus, for a drainage basin with an area A, we calculate $\mathrm{Pe} = (K/D)(3A)^{m+\frac{1}{2}}$. We used drainage area to calculate equivalent basin lengths rather than measuring basin length directly because drainage area is an integrated measure of basin size that is less sensitive to differences in basin shape.

In addition to this quantitative test of the proposed mechanisms for the development of tributary networks, visual inspection of the topography provides a qualitative means of identifying evidence that these mechanisms have operated in a landscape. For example, Supplementary Fig. 3 shows several adjacent drainage basins that appear to have undergone the instabilities illustrated in Figs 2c and 3.

Landscape evolution model. The landscape evolution model is a modified version of the Tadpole model[21,23], which solves an equation for the time evolution of an elevation surface, $z(x, y)$, derived[13,23,39] from conservation of mass and rate laws for soil creep and channel incision,

$$\frac{\partial z}{\partial t} = D\nabla^2 z - KA^m|\nabla z| + E \quad (2)$$

where z is elevation, t is time, D is the soil transport coefficient, A is drainage area, K and m are constants, and E is the rate of boundary lowering. Elevation is measured relative to the lowering boundary, such that E appears in equation (2) as a surface uplift rate. The linear diffusion term is based on the theoretical expectation[40,41], supported by field measurements[42–47], that soil creep flux on hillslopes with gentle to moderate gradients is driven by isotropic disturbance (due to animal burrowing, for example) and gravitational settling, such that soil flux is proportional to the topographic gradient. The nonlinear kinematic wave term is based on studies of erosional channels[28,48–50] suggesting that channel incision rate is proportional to the rate of energy expenditure by the flow of water[51], or 'stream power', per unit area of the bed under normal flow. A term with the same form—that is, a power law dependence of channel incision rate on drainage area and slope—is obtained if incision rate is instead assumed to be proportional to shear stress[52].

The linear diffusion term describes the smoothing effect of slope-dependent soil creep, and the nonlinear kinematic wave term describes how changes in elevation at the boundaries propagate upslope through the landscape, including a strong positive feedback in valley incision through the dependence on drainage area. The boundary lowering (or, equivalently, uplift relative to the boundaries), E, drives the development of the landscape by steepening the topography. The competition between these effects gives rise to a landscape with smooth, concave down ridgelines and sharper, concave-up valleys. As noted in the main text, the Péclet number describes the relative magnitudes of the soil creep and channel incision terms[23].

The use of a continuum model with constant coefficients implicitly averages in space and time over many erosion and transport events, which would be difficult to describe individually. For example, this model assumes that channel incision and soil creep can occur in the same location, in a time-averaged sense, and is therefore appropriate for low-order drainage basins in which episodes of channelization are interspersed with periods of diffusive infilling (Supplementary Fig. 4). The modelling approach employed here makes it possible to explore the main controls on landscape form in terms of a few parameters.

Equation (2) was solved numerically on a 300 × 100 ($N_x \times N_y$) regular grid with $\Delta x, \Delta y = 5$ m using a finite difference method[23]. The grid was subject to a constant lowering of the y boundaries intended to mimic a set of parallel, incising channels. The x boundaries were periodic, such that the topography repeats with a period equal to the length of the domain in the x direction. Experiments began with an initial surface of uncorrelated Gaussian noise with a variance of 1 m^2, and continued until the topography reached a dynamic equilibrium in which all points were lowering at the same rate. In each experiment, incipient drainage basins formed at the lowering y boundaries and advanced towards the interior of the grid in a direction perpendicular to the y boundaries. A central drainage divide formed where the basins advancing in opposite directions met roughly halfway between the y boundaries. Supplementary Fig. 5 shows steady-state solutions for three experiments.

©2012 Macmillan Publishers Limited. All rights reserved

We varied the Péclet number in the model by setting $m = 0.5$ and changing the ratio K/D. The length scale L was defined as half of the length of the domain in the y direction, which is the approximate length of drainage basins that extend from the central drainage divide to one of the lowering boundaries. In each model solution, we identified drainage basin outlets as points adjacent to one of the lowering boundaries with $\nabla^2 z \geq 0.005\,\mathrm{m}^{-1}$, measured the drainage area at each outlet, and normalized the areas by L^2. While the mean characteristics of drainage basins at steady state for a given Péclet number are independent of initial conditions, the characteristics of individual basins are sensitive to initial conditions, and vary about the mean[53]. To better characterize the size distribution of drainage basins for a given Pe, we performed an ensemble of 1,600 simulations with identical parameters and boundary conditions, but different initial surfaces. A probability density map of the resulting population of more than 60,000 drainage basins as a function of drainage basin size and Péclet number reveals a transition from a unimodal to a bimodal size distribution over the interval $250 < \mathrm{Pe} < 300$ (Fig. 2).

Cosmogenic nuclides. We estimated long-term erosion rates in AP and GM by measuring the concentration of cosmogenic ^{10}Be in quartz grains in stream sediment, following an established procedure[54]. This yields erosion rates that are spatially averaged over the sampled drainage basins and temporally averaged over the characteristic time of ^{10}Be accumulation in the sampled quartz, which is typically 10^3–10^5 yr in most eroding landscapes. We collected sediment samples from three drainage basins in AP and two in GM in 2009 and 2010. All sampled basins have quartz-rich lithologies (sandstone in AP, sandstone and quartzite conglomerate in GM). We separated and dissolved quartz from each sample following a standard procedure[55] and isolated ^{10}Be using cation exchange[56]. ^{10}Be/^{9}Be ratios were measured with Accelerator Mass Spectrometry at PRIME Lab, Purdue University, in February 2011. The mean location and elevation of each drainage basin were used to determine ^{10}Be production rates[57]. For small drainage basins like those analysed here, the uncertainty introduced by using a single location and elevation to approximate the production rate is typically much smaller than uncertainties associated with other assumptions required to calculate basin-averaged erosion rates[57]. A correction factor accounting for topographic shielding from cosmic rays[57] was calculated at each pixel in a 4 m per pixel version of the laser altimetry map of GM, and the mean value for each drainage basin was used. The shielding correction at all of the AP sites was found to be negligible.

Because the sediments that make up GM are young, and might therefore have been exposed at the surface recently, we corrected the ^{10}Be concentrations in the GM samples by subtracting the inherited concentration measured in three shielded samples with the same lithology. The shielded samples were collected in 2002 from recently excavated drill platforms near the 2009–10 surface sample locations. When the samples were originally buried to depths much deeper than 1 m, they were shielded from subsequent production and the ^{10}Be concentration was altered only by radioactive decay. The shielded samples were processed at the University of California, Berkeley, and ^{10}Be/^{9}Be ratios were measured with Accelerator Mass Spectrometry at Lawrence Livermore National Laboratory in 2005. The mean ^{10}Be concentration of the shielded samples was subtracted from the ^{10}Be concentrations of the surface samples to determine the ^{10}Be concentration accumulated during recent exposure (Supplementary Table 1). Given the close vertical proximity of the shielded samples and the 1.36 Myr half-life of ^{10}Be, we interpret the difference in ^{10}Be concentration in the shielded samples to reflect slightly different source and transport histories rather than different durations of burial.

^{10}Be concentrations of the surface samples at both sites were converted into erosion rates using the CRONUS calculator[57], version 2.2. Measured quantities used in this calculation, and the resulting erosion rates, are summarized in Supplementary Table 1. The uniform relief of both landscapes and the consistency of the erosion rates among sampling locations suggest that these rates are representative of the surrounding landscape. We therefore average the erosion rates to arrive at a single rate for each landscape: $92 \pm 5\,\mathrm{t\,km^{-2}\,yr^{-1}}$ for AP, and $206 \pm 27\,\mathrm{t\,km^{-2}\,yr^{-1}}$ for GM. The uncertainties were taken to be the larger of the standard error of the mean of the site-specific rates and the pooled site-specific uncertainties.

For comparison with the model predictions, these mass removal rates must be converted to surface erosion rates with units of $[\mathrm{L\,T^{-1}}]$. Dividing by measured soil densities of $1{,}660 \pm 110\,\mathrm{kg\,m^{-3}}$ in AP and $1{,}400 \pm 100\,\mathrm{kg\,m^{-3}}$ in GM yields surface erosion rates of $55 \pm 5\,\mathrm{m\,Myr^{-1}}$ in AP and $147 \pm 22\,\mathrm{m\,Myr^{-1}}$ in GM. This calculation assumes that chemical mass removal by dissolution is negligible.

Calculation of K and D. At steady state ($\partial z/\partial t = 0$), the surface erosion rate at any location equals the boundary lowering rate, and equation (2) reduces to:

$$-E = D\nabla^2 z - KA^m|\nabla z| \tag{3}$$

On hilltops, where drainage area and slope are small, $A^m|\nabla z| \approx 0$, and

$$D = -\frac{E}{\nabla^2 z_\mathrm{h}} \tag{4}$$

where $\nabla^2 z_\mathrm{h}$ is the Laplacian of elevation on hilltops. We used equation (4) to estimate D for AP and GM, using the surface erosion rates measured with cosmogenic nuclides as an estimate of E, and the hilltop Laplacian measured in ref. 21 (Supplementary Table 2). The uniform value of the Laplacian over each hillslope supports the steady-state assumption in equation (3). Given D and an estimate of D/K (ref. 21), it is straightforward to calculate K. The units of K depend on the value of m. To facilitate comparisons among different landscapes where m can vary, we compare the quantity KA_ref^m, where A_ref is a reference drainage area, here taken to be $10^4\,\mathrm{m^2}$. The estimated m values for AP and GM are very similar (Supplementary Table 2), so the difference in KA_ref^m is due almost entirely to the difference in K. Note that KA_ref^m is faster than the actual channel incision rate, which also depends on slope.

30. Mitášová, H. & Hofierka, J. Interpolation by regularized spline with tension: II. Application to terrain modeling and surface geometry analysis. *Math. Geol.* **25,** 657–669 (1993).
31. Peckham, S. D. in *Geomorphometry 2011* (eds Hengl, T. Evans, I. S., Wilson, J. P. & Gould, M.) 27–30 (2011); available at http://geomorphometry.org/Peckham2011a (2011).
32. Lashermes, B., Foufoula-Georgiou, E. & Dietrich, W. E. Channel network extraction from high resolution topography using wavelets. *Geophys. Res. Lett.* **34,** L23S04, http://dx.doi.org/10.1029/2007GL031140 (2007).
33. Passalacqua, P., Do Trung, T., Foufoula-Georgiou, E., Sapiro, G. & Dietrich, W. E. A geometric framework for channel network extraction from lidar: nonlinear diffusion and geodesic paths. *J. Geophys. Res.* **115,** F01002, http://dx.doi.org/10.1029/2009JF001254 (2010).
34. Tarboton, D. G. A new method for the determination of flow directions and upslope areas in grid digital elevation models. *Wat. Resour. Res.* **33,** 309–319 (1997).
35. Jenson, S. K. & Domingue, J. O. Extracting topographic structure from digital elevation data for geographic information system analysis. *Photogramm. Eng. Remote Sensing* **54,** 1593–1600 (1988).
36. Gonzalez, R. C., Woods, R. E. & Eddins, S. L. *Digital Image Processing Using MATLAB* (Pearson Prentice Hall, 2004).
37. Dietrich, W. E. & Dunne, T. in *Channel Network Hydrology* (eds Beven, K. & Kirkby, M. J.) 175–219 (Wiley & Sons, 1993).
38. Hack, J. T. Studies of longitudinal stream profiles in Virginia and Maryland. *Prof. Pap. US Geol. Surv.* **294-B,** 1–97 (1957).
39. Tucker, G. E. & Slingerland, R. Predicting sediment flux from fold and thrust belts. *Basin Res.* **8,** 329–349 (1996).
40. Culling, W. E. H. Analytical theory of erosion. *J. Geol.* **68,** 336–344 (1960).
41. Culling, W. E. H. Soil creep and the development of hillside slopes. *J. Geol.* **71,** 127–161 (1963).
42. Nash, D. Morphologic dating of degraded normal fault scarps. *J. Geol.* **88,** 353–360 (1980).
43. Hanks, T. C., Bucknam, R. C., Lajoie, K. R. & Wallace, R. E. Modification of wave-cut and faulting-controlled landforms. *J. Geophys. Res.* **89,** 5771–5790 (1984).
44. Rosenbloom, N. A. & Anderson, R. S. Hillslope and channel evolution in a marine terraced landscape, Santa Cruz, California. *J. Geophys. Res.* **99,** 14013–14029 (1994).
45. Monaghan, M. C., McKean, J., Dietrich, W. & Klein, J. ^{10}Be chronometry of bedrock-to-soil conversion rates. *Earth Planet. Sci. Lett.* **111,** 483–492 (1992).
46. McKean, J. A., Dietrich, W. E., Finkel, R. C., Southon, J. R. & Caffee, M. W. Quantification of soil production and downslope creep rates from cosmogenic ^{10}Be accumulations on a hillslope profile. *Geology* **21,** 343–346 (1993).
47. Small, E. E., Anderson, R. S. & Hancock, G. S. Estimates of the rate of regolith production using ^{10}Be and ^{26}Al from an alpine hillslope. *Geomorphology* **27,** 131–150 (1999).
48. Seidl, M. A., Dietrich, W. E. & Kirchner, J. W. Longitudinal profile development into bedrock: an analysis of Hawaiian channels. *J. Geol.* **102,** 457–474 (1994).
49. Stock, J. D. & Montgomery, D. R. Geologic constraints on bedrock river incision using the stream power law. *J. Geophys. Res.* **104,** 4983–4994 (1999).
50. Snyder, N. P., Whipple, K. X., Tucker, G. E. & Merritts, D. J. Channel response to tectonic forcing: field analysis of stream morphology and hydrology in the Mendocino triple junction region, northern California. *Geomorphology* **53,** 97–127 (2003).
51. Seidl, M. A. & Dietrich, W. E. The problem of channel erosion into bedrock. *Catena* **23,** 101–124 (1992).
52. Howard, A. D. & Kerby, G. Channel changes in badlands. *Bull. Geol. Soc. Am.* **94,** 739–752 (1983).
53. Perron, J. T. & Fagherazzi, S. The legacy of initial conditions in landscape evolution. *Earth Surf. Process. Landf.* **37,** 52–63 (2012).
54. Granger, D., Kirchner, J. & Finkel, R. Spatially averaged long-term erosion rates measured from in situ-produced cosmogenic nuclides in alluvial sediment. *J. Geol.* **104,** 249–257 (1996).
55. Kohl, C. P. & Nishiizumi, K. Chemical isolation of quartz for measurement of in-situ-produced cosmogenic nuclides. *Geochim. Cosmochim. Acta* **56,** 3583–3587 (1992).
56. Ditchburn, R. G. & Whitehead, N. E. The separation of ^{10}Be from silicates. In *Proc. Third Workshop of the South Pacific Environmental Radioactivity Association* 4–7 (1994).
57. Balco, G., Stone, J. O., Lifton, N. A. & Dunai, T. J. A complete and easily accessible means of calculating surface exposure ages or erosion rates from ^{10}Be and ^{26}Al measurements. *Quat. Geochronol.* **3,** 174–195 (2008).

©2012 Macmillan Publishers Limited. All rights reserved